Journal of Solid State Chemistry 182 (2009) 236–239

Contents lists available at ScienceDirect

Journal of Solid State Chemistry

journal homepage: www.elsevier.com/locate/jssc

Morphology modulated growth of bismuth tungsten oxide nanocrystals

Shushan Yao [a], Jiyong Wei [a,b], Baibiao Huang [a,*], Shengyu Feng [b], Xiaoyang Zhang [a], Xiaoyan Qin [a], Peng Wang [a], Zeyan Wang [a], Qi Zhang [a], Xiangyang Jing [a], Jie Zhan [a]

[a] State Key Lab of Crystal Materials, Shandong University, Jinan 250100, China
[b] Chemistry and Chemical Engineering College, Shandong University, Jinan 250100, China

ARTICLE INFO

Article history:
Received 7 April 2008
Received in revised form
7 July 2008
Accepted 23 September 2008
Available online 8 October 2008

Keywords:
Morphology
Nanomaterials
Photocatalyst
Crystal growth

ABSTRACT

Two kinds of bismuth tungsten oxide nanocrystals were prepared by microwave hydrothermal method. The morphology modulation of nanocrystals synthesized with precursor suspension's pH varied from 0.25 (strong acid) to 10.05 (base) was studied. The 3D flower like aggregation of Bi_2WO_6 nanoflakes was synthesized in acid precursor suspension and the nanooctahedron crystals of $Bi_{3.84}W_{0.16}O_{6.24}$ were synthesized in alkalescent precursor. The dominant crystal is changed from Bi_2WO_6 to $Bi_{3.84}W_{0.16}O_{6.24}$ when the precursor suspension changes from acid to alkalescence. The growth mechanisms of Bi_2WO_6 and $Bi_{3.84}W_{0.16}O_{6.24}$ were attributed to the different solubility of WO_4^{2-} and $[Bi_2O_2]^{2+}$ in precursor suspensions with various pH. For the decomposition of Rhodamine B (RhB) under visible light irradiation ($\lambda > 400$ nm), different morphology of Bi_2WO_6 crystal samples obtained by microwavesolvothermal process showed different photocatalytic activity.

1. Introduction

Bismuth tungsten oxide, is the simplest member of the Aurivillius family of layered perovskites, which are structurally comprised of alternating perovskite-like slab of WO_6 and $[Bi_2O_2]^{2+}$ layers. It has been found that Bi_2WO_6 possess some interesting applications, a well-known ferroelectric material [1], an oxygen ion conductor [2], a potential candidate to be used as catalyst in the CO to CO_2 oxidation [3], a substance for the photocatalytic decomposition of organic contaminants [4–6]. The Bi_2WO_6 sample has a suitable valence band that meets the potential level of oxidizing the organic contaminants. bismuth tungsten oxide material system was recently studied as visible light photocatalysts [7–13,22–25]. Tang [4] have reported that Bi_2WO_6 had photocatalytic activities for O_2 evolution/water splitting and could degrade the organic compound ($CHCl_3$ and CH_3CHO) under visible light irradiation. Wang et al. [14] recently studied the effects of surfactant, calcinations and pH value (pH value range from 1.5 to 7.5) on nano and microstructure of Bi_2WO_6.

As for photocatalysts, nanoparticles usually have high photocatalytic activities because of their special morphologies, high surface areas and so on. Experimental observations and theoretical calculations also indicate that anisotropic metal nanostructures exhibit shape-dependent optical properties [15]. Therefore morphology control of semiconductor and metal oxide nanocrystals become very important in synthesis of nanomaterials [16–19]. Different synthetic approaches may give raise to particular properties due to possible variation of surface morphology and structure. Microwave hydrothermal method [20] is clean and efficient method for materials preparation. Ling et al. [21] recently successfully synthesized Nanocrystalline Bi_2WO_6 photocatalyst with nanosheet morphology was by a microwave solvothermal process, but the effect of pH value of precursor suspensions on the Bi_2WO_6 nanostructure and photocatalysis activity did not mentioned.

We have synthesized two kinds of bismuth tungsten oxide nanocrystals by microwave hydrothermal method, and modulated the morphology by precursor suspension's pH variation from strong acid (0.25) to base (10.05), and discussed the growth mechanism.

2. Experimental details

The preparation of the precursor suspensions consists of four steps: (1) preparation of 0.2 mol/l Bi^{3+}: added 50 mmol $Bi(NO_3)_3 \cdot 5H_2O$ into 1.2 mol/l HNO_3, diluted to 250 ml; (2) Preparation of 0.1 mol/l Na_2WO_4: added 25 mmol H_2WO_4 to slightly excessive NaOH solution, diluted to 250 ml; (3) 0.1 mol/l Na_2WO_4 solution was added dropwise into 0.2 mol/l Bi^{3+} solution, stirring with magneton stirrer; (4) NaOH solution was added to modulate the pH value from acid to alkaline.

* Corresponding author. Fax: +86 531 88365969.
E-mail address: bbhuang@sdu.edu.cn (B. Huang).

0022-4596/$ - see front matter © 2008 Elsevier Inc. All rights reserved.
doi:10.1016/j.jssc.2008.09.016

Then the reaction mixture was sealed in a 100 mL teflon-lined digestion vessel. The vessel was enclosed by a safety shield and heated at 180 °C for 1 h using a microwave synthesizer. A pale yellow suspension formed after the microwave hydrothermal treatment. The products were washed with deionized water and then were dried at 80 °C before characterization.

The products were characterized with X-ray diffraction (XRD, Cu$K\alpha$, D/max-ra X-ray) to identify the crystal phases, the crystal morphology was characterized by surface scanning electron microscopy (SEM, JEOL JSM6700F) and transmission electron microscopy(TEM, HITACH H-600).

The visible light photocatalytic activities of Bi_2WO_6 nanoparticles were valuated by the decomposition of rhodamine B (RhB) in water under visible light irradiation. The optical system for the photocatalytic reaction was composed of a Xe arc lamp (500 W, Philips Electronics) and a cutoff filter ($\lambda > 400$ nm). The photocatalytic reaction procedures are similar to that in the Ref. [22]. RhB solutions (100 mL, 20 mg L^{-1}) containing Bismuth tungsten oxide nanocrystals (100 mg) were put in a cylindrical glass vessel. Before the light was turned on, the solution was first ultrasonicated for 10 min, and then stirred for 10 min to ensure equilibrium between the catalyst and the solution. Three milliliter of samples were taken at given time intervals and separated through centrifugation (2000 rpm, 15 min). The degraded solution was analyzed by a Varian Cary 50 Scan UV-visible spectrophotometer.

3. Results and discussion

3.1. Crystal phase and morphology characterization

Powder samples prepared were characterized by XRD, as shown in Fig. 1. The XRD data recognized the crystal structure as orthorhombic symmetry Bi_2WO_6 crystal phase (PDF number: 39-0256) from pH ranges of 0.25–7.02, whereas emerged the second crystal phases of cubic symmetry $Bi_{3.84}W_{0.16}O_{6.24}$ crystal phase (PDF number: 43-447) from pH ranges above 9. The XRD spectrum's peak intensity of sample prepared from acidity precursor suspensions becomes stronger. The intensity of the strongest (1 3 1) peak changed from about 150 to about 3000 as pH varied from 0.25 to 7.02, indicating an increase in crystallite size and an enhance in crystallinity perfection. The intensity ratios of the strongest peak (1 3 1) and the next strongest peak (0 6 0) vary as the pH value changed from 0.25 to 7, which implies the morphology changes of the nanocrystal. The crystal has special anisotropic growth along the (0 0 1) plane. These results can be attributed to the orthorhombic structure of the nanocrystal, which is proved by further study by SEM and TEM.

Morphology modulation of the Bi_2WO_6 nanoflake via pH was characterized by SEM and TEM. As the precursor suspension was in strong acidity (with pH value of 0.25, Fig. 2A), nanoflakes with poor morphology and crystallinity were observed from SEM, which aggregated like cabbages, and nearly hollow aggregations were observed through TEM (Fig. 3A). Electron diffraction scatter spot of the nanoflakes showed the orthorhombic symmetry, which was in accord with the XRD spectrum characterization (PDF number: 39-0256). As the precursor suspension was in medium acidity, with pH value range from 2 (Fig. 2B) to 4.05 (Fig. 2C), the crystallinity of nanoflake like crystals was enhanced and the morphology of Bi_2WO_6 observed from SEM was like nanoroses, whereas from TEM near unity hollow ball like aggregations of nanoflakes (with aggregation diameter about 2 μm) was observed from TEM photo of Fig. 3B (pH 1.98) and Fig. 3C (pH 4.05). The diameter unity and morphology perfection were enhanced as the pH value varied from 1.98 to 4.05. As the pH value was neuter, nanoflakes of Bi_2WO_6 were randomly piled up with no typical aggregation observed from SEM photo (see Fig. 2D, pH 7.02), but the TEM characterization (Fig. 3D) showed the non-hollow aggregation of Bi_2WO_6 crystal.

As the pH value of precursor suspensions reached to alkalescence (Figs. 2E and 3E, with pH 9), a second crystal phase of $Bi_{3.84}W_{0.16}O_{6.24}$ appeared together with Bi_2WO_6 thick nanoflakes. The morphology of $Bi_{3.84}W_{0.16}O_{6.24}$ was ball-like with poor crystallinity observed from SEM (Fig. 2E), but the crystallinity of Bi_2WO_6 phase was nearly perfect with nanobrick-like

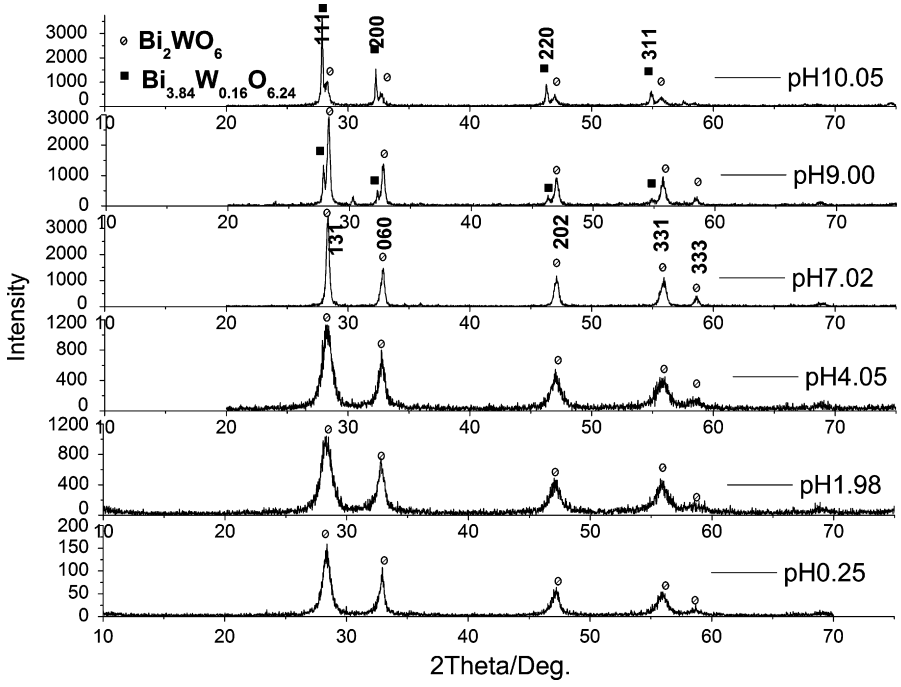

Fig. 1. XRD characterization of bismuth tungsten oxide nanocrystals synthesized in precursor suspensions with different pH.

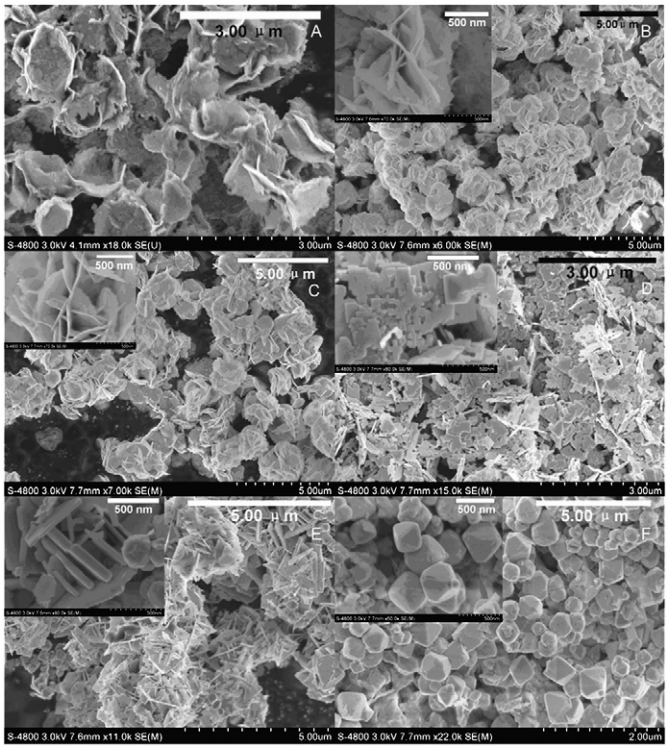

Fig. 2. SEM characterization of synthesized bismuth tungsten oxide nanomaterials from precursor suspensions of different pH: (A) 0.25; (B) 1.98; (C) 4.05; (D) 7.02; (E) 9.00; (F) 10.05.

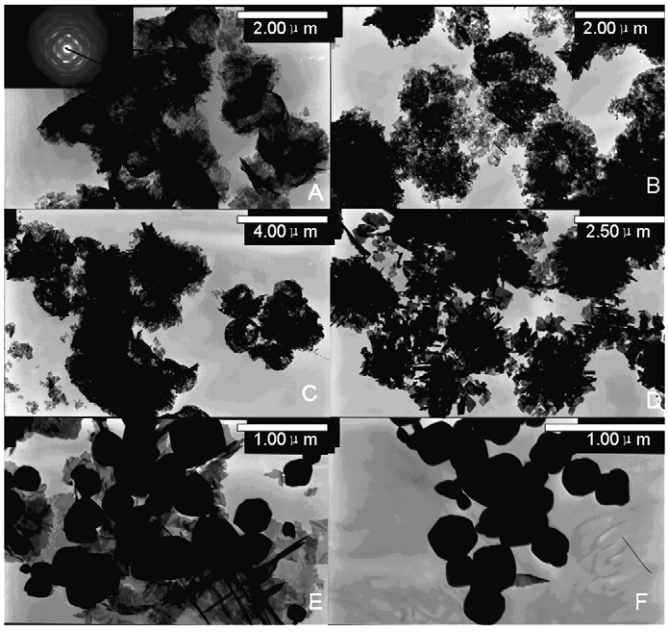

Fig. 3. TEM characterization of synthesized bismuth tungsten oxide nanomaterials from precursor suspensions of different pH: (A) 0.25; (B) 1.98; (C) 4.05; (D) 7.02; (E) 9.00; (F) 10.05.

(about 100 nm thick), which aggregated to construct architectures of several micrometers. Morphology of the whole material is mainly constructed by nanobrick like of Bi_2WO_6 crystals and ball-like nanocrystals of $Bi_{3.84}W_{0.16}O_{6.24}$ phase.

While the pH value of precursor reached to 10.05 (Figs. 2F and 3F), the dominant crystal phase changed to $Bi_{3.84}W_{0.16}O_{6.24}$. The $Bi_{3.84}W_{0.16}O_{6.24}$ crystals with good morphology were observed, the size of crystals is several hundreds nanometers. The Bi_2WO_6 phase degenerated to amorphous ball-like nanocrystals dotting on $Bi_{3.84}W_{0.16}O_{6.24}$ octahedron crystals.

3.2. Growth mechanism discussion

The growth mechanism of bismuth tungsten oxide is proposed a hydrothermal ripening process [5]: a highly supersaturated solution was adopted, and amorphous fine particles acted as the precursor for the synthesis of crystal. The different morphology of bismuth tungsten oxide nanomaterials result from the different solubility of $(WO_4)^{2-}$ and $(Bi_2O_2)^{2+}$ in precursor suspensions with various pH.

Bi_2WO_6 crystals consist of alternating $(Bi_2O_2)^{2+}{}_n$ layers and perovskite like $(WO_4)^{2-}{}_n$ layers, stacking along the c axis, and the high intrinsic anisotropic growth in various tungstates is mainly due to the octahedral $(WO_4)^{2-}{}_n$ chains. The small solubility of $(WO_4)^{2-}_n$ in acid solutions results in relatively slow crystal growth rates. As pH varies from 0.25 to about 4.05, the concentration of OH^- is much lower than that of H^+, which refrains the hydrolysis of $(Bi_2O_2)^{2+}$ and decrease the crystal growth rate of Bi_2WO_6, so the fast nucleation and aggregation rates of Bi_2WO_6 nanoflakes result in the 3D spherical flower-like aggregation. As pH value increased to 7, the concentration of OH^- and H^+ is about the same. The hydrolysis of $(Bi_2O_2)^{2+}$ is mediate, but more WO_4^{2-} dissolve in precursor suspensions, so the amount devoted to crystal growth is decreased. The anisotropic growth of Bi_2WO_6 is refrained due to the decreasing of the amount of WO_4^{2-} devoted to crystal growth. So the crystal growth rates of Bi_2WO_6 nanoflakes is not enhanced evidently. As the pH value reaches 9, the hydrolysis reaction of $(Bi_2O_2)^{2+}$ is enhanced but the concentration of WO_4^{2-} in solution is also greatly enhanced and very few amount devoted for crystal growth, so the second phase $Bi_{3.84}W_{0.16}O_{6.24}$ appears due to the precipitation of $[Bi_2O_2]^{2+}$ and high solubility of WO_4^{2-} in alkaline solution, thus the Bi_2WO_6 and the $Bi_{3.84}W_{0.16}O_{6.24}$ phase coexists and competition, whereas at pH 9, the crystal phase of Bi_2WO_6 is the dominate phase. As the pH value reaches 10.05, the $Bi_{3.84}W_{0.16}O_{6.24}$ phase is the dominate phase, because of high solubility of WO_4^{2-} and very small amount devote to crystal growth, the anisotropic growth of crystal is refrained , so the $Bi_{3.84}W_{0.16}O_{6.24}$ phase is nearly perfect octahedron crystals.

3.3. Photocatalytic activity evaluation

Photocatalytic activities of the samples are evaluated by the degradation of RhB in the aqueous solution under visible light irradiation. Temporal changes in the concentration of RhB are monitored by examining the variations in maximal absorption in UV–vis spectra at 554 nm. The photodegradation efficiencies of RhB were evaluated by the different photocatalysts under visible-light illumination ($\lambda > 400$ nm).

The concentration of rhodamine species was simply determined by the maximum absorption measurement because the molar extinction coefficients of different rhodamine species were in a narrow range. The relationship was revealed by the plots of the C/C_0 (C was the concentration of RhB at the irradiation time t and C_0 was the concentration in the adsorption equilibrium on Bi_2WO_6 before irradiation) vs irradiation time (t).

Fig. 4 shows the temporal evolution of the spectral changes of the RhB mediated by photocatalysts A (Bi_2WO_6 nanoflakes synthesized with precursor suspension pH 0.25). With the photocatalytic degradation of RhB, the absorption peak at 554 nm blue-shifts and broadens at the same time. This agrees well with the report of Zhao and coworkers in the TiO2/RhB process [5]. According to their report, the blue-shift of absorption

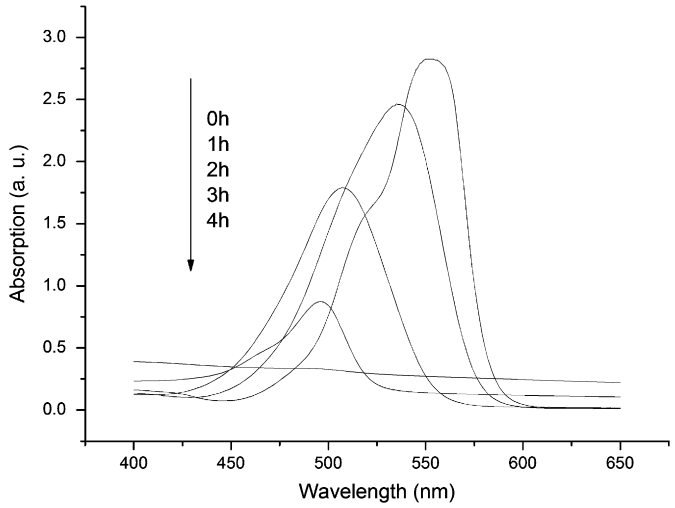

Fig. 4. The temporal evolution of the spectral changes of the RhB mediated by photocatalysts A (Bi_2WO_6 nanoflakes synthesized with precursor suspension pH 0.25).

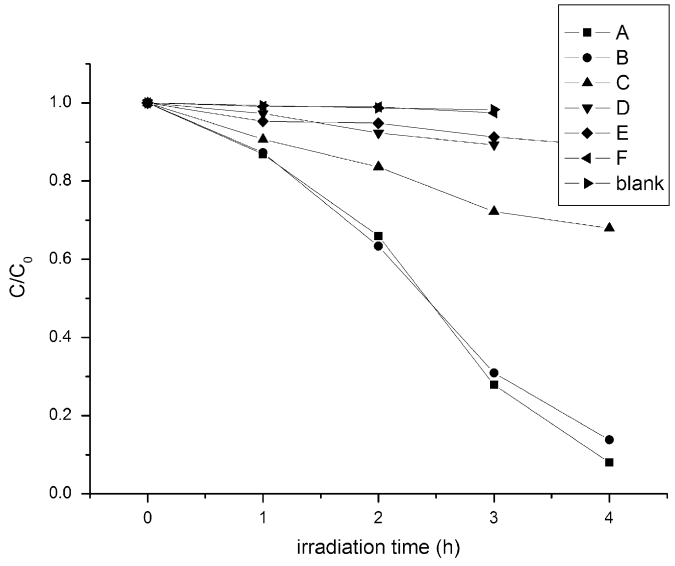

Fig. 5. Photodegradation efficiencies of RhB mediated by the different photocatalysts (A: pH 0.25; B: pH 1.98; C: pH 4.05; D: pH 7.02; E: pH 9.00; F: pH 10.05;) as well as without photocatalyst (Blank: the blank test) under visible-light irradiation ($\lambda > 400$ nm).

band is caused by de-ethylation of RhB because of the attack by one of the active oxygen species on the *N*-ethyl group. When the de-ethylated process is fully completed, the absorption band shifts to 490 nm at wavelength and RhB turns to rhodamine. Then rhodamine is gradually decomposed due to the further destruction of the conjugated structure.

Fig. 5 shows the photodegradation efficiencies of RhB mediated by the different photocatalysts (A: pH 0.25; B: pH 1.98; C: pH 4.05; D: pH 7.02; E: pH 9.00; F: pH 10.05) as well as without photocatalyst (blank: the blank test) under visible-light irradiation ($\lambda > 400$ nm), respectively. We could note that RhB could degrade naturally under visible-light irradiation, but the degradation rate was extremely slow (shown in Fig. 5 blank). As the precursor suspension was in acidity, photocatalysis activity of Bi_2WO_6 nanocrystals shows its dependence on the pH value. The higher the pH value is, the lower the photocatalyst activity of the sample performed. It is mainly attributed to a better crystalline phase and is consistent with the XRD and TEM results. As the pH value of precursor suspensions reached to alkalescence (shown in Fig. 5E and F), degradation rate of RhB was extremely slow because of the appearance of $Bi_{3.84}W_{0.16}O_{6.24}$ nanocrystals.

4. Conclusions

The morphology and aggregation's evolution of Bi_2WO_6 nanoflakes were studied. The crystal transition of Bi_2WO_6 nanoflakes to nearly perfect octahedron $Bi_{3.84}W_{0.16}O_{6.24}$ nanocrystals was successfully carried out by modulating the pH of precursor suspensions from 0.25 (strong acidity) to 10.05 (alkalescence). The growth mechanism of bismuth tungsten oxide nanomaterials was proposed. The different morphology of bismuth tungsten oxide nanomaterials was attributed to the solubility of WO_4^{2-} and $[Bi_2O_2]^{2+}$ in precursor suspensions with various pH. The Bi_2WO_6 nanoplates performed high photocatalytic activities under visible light irradiation. The photocatalytic evaluation, via the decomposition of Rhodamine B (RhB) under visible light irradiation ($\lambda > 420$ nm), reveals that nanocrystalline Bi_2WO_6 samples obtained under different conditions exhibit different photocatalytic activities which depend on pH value of precursor suspensions.

Acknowledgments

This work is financially supported by a research grant from the National Basic Research Program of China (No. 2007CB613302) and the National Natural Science Foundation of China (Nos. 50721002, 10774091 and 50672052).

References

[1] P.S. Berdonosov, D.O. Charkin, V.A. Dolgikh, S.Y. Stefanovich, R.I. Smith, P. Lightfoot, J. Solid State Chem. 177 (2004) 2632–2634.
[2] K. Ishikawa, T. Watanabe, H. Funakubo, Thin Solid Films 392 (2001) 128–133.
[3] R. Rangel, P. Bartolo-Perez, A. Gomez-Cortes, G. Diaz, D.H. Galvan, Surf. Rev. Lett. 9 (2002) 1779–1783.
[4] J.W. Tang, Z.G. Zou, J.H. Ye, Catal. Lett. 92 (2004) 53–56.
[5] C. Zhang, Y.F. Zhu, Chem. Mater. 17 (2005) 3537–3545.
[6] J.G. Yu, J.F. Xiong, B. Cheng, Y. Yu, J.B. Wang, J. Solid State Chem. 178 (2005) 1968–1972.
[7] J. Wu, F. Duan, Y. Zheng, Y. Xie, J. Phys. Chem. C. 111 (2007) 12866–12871.
[8] J.W. Tang, J.H. Ye, J. Mater. Chem. 15 (2005) 4246–4251.
[9] L.S. Zhang, W.H. Wang, Z.G. Chen, L. Zhou, H.L. Xu, W. Zhu, J. Mater. Chem. 17 (2007) 2526–2532.
[10] J. Li, X. Zhang, Z. Ai, F. Jia, L. Zhang, J. Lin, J. Phys. Chem. C. 111 (2007) 6832–6836.
[11] H. Fu, C. Pan, W. Yao, Y. Zhu, J. Phys. Chem. B. 109 (2005) 22432–22439.
[12] A.P. Finlayson, V.N. Tsaneva, L. Lyons, M. Clark, B.A. Glowacki, Phys. Status Solidi (a) 203 (2006) 327–335.
[13] Kudo, S. Hijii, Chem. Lett. 28 (1999) 1103–1104.
[14] L. Zhang, W. Wang, L. Zhou, H. Xu, Small 3 (2007) 1618–1625.
[15] R.C. Jin, Y.W. Cao, C.A. Mirkin, K.L. Kelly, G.C. Schatz, J.G. Zheng, Science 294 (2001) 1901–1903.
[16] W. Jun, J.S. Choi, J. Cheon, Angew. Chem. Int. Ed. 45 (2006) 3414–3439.
[17] Y.W. Jun, J.W. Seo, S.J. Oh, J. Cheon, Coord. Chem. Rev. 249 (2005) 1766–1775.
[18] Y. W Jun, J.H. Lee, J.S. Choi, J.W. Cheon, J. Phys. Chem. B. 109 (2005) 14795–14806.
[19] S.H. Choi, E.G. Kim, J. Park, K. An, N. Lee, S.C. Kim, T. Hyeon, J. Phys. Chem. B. 109 (2005) 14792–14794.
[20] K.J. Rao, B. Vaidhyanathan, M. Ganguli, P.A. Ramakrishnan, Chem. Mater. 11 (1999) 882–895.
[21] L. Wu, J.H. Bi, Z.H. Li, X.X. Wang, X.Z. Fu, Catal. Today 131 (2008) 15–20.
[22] J.G. Yua, J.F. Xiong, B. Cheng, Y. Yu, J.B. Wang, J. Solid State Chem. 178 (2005) 1968–1972.
[23] S.C. Zhang, C. Zhang, Y. Man, Y.F. Zhu, J. Solid State Chem. 179 (2006) 62–69.
[24] J.W. Tang, Z.G. Zou, J.H. Ye, Catal. Lett. 92 (2004) 53–56.
[25] F. Amano, K. Nogami, R. Abe, B. Ohtani, Chem. Lett. 36 (2007) 1314–1315.